Thermonuclear ^{19}F(p,α_0)^{16}O reaction rate*

Jian-Jun He(何建军)[1;1)] Ivano Lombardo[2] Daniele Dell'Aquila[3,4]
Yi Xu(徐毅)[5,6] Li-Yong Zhang(张立勇)[1] Wei-Ping Liu(柳卫平)[7]

[1] Key Laboratory of Optical Astronomy, National Astronomical Observatories, Chinese Academy of Sciences, Beijing 100012, China
[2] INFN - Sezione di Catania, via S. Sofia, I-95123, Catania, Italy
[3] Dip. di Fisica, Univ. di Napoli Federico II, via Cintia, I-80126, Napoli, Italy
[4] INFN - Sezione di Napoli, via Cintia, I-80126, Napoli, Italy
[5] Extreme Light Infrastructure - Nuclear Physics, 30 Reactorului Street, P.O. Box MG-6, 077125 Magurele, jud. Ilfov, Romania
[6] Nuclear Physics Institute, Czech Academy of Sciences, Řež, 25068, Czech Republic
[7] China Institute of Atomic Energy, P. O. Box 275(10), Beijing 102413, China

Abstract: The thermonuclear ^{19}F(p,α_0)^{16}O reaction rate in the temperature region 0.007–10 GK has been derived by re-evaluating the available experimental data, together with the low-energy theoretical R-matrix extrapolations. Our new rate deviates by up to about 30% compared to the previous results, although all rates are consistent within the uncertainties. At very low temperature (e.g. 0.01 GK) our reaction rate is about 20% lower than the most recently published rate, because of a difference in the low energy extrapolated S-factor and a more accurate estimate of the reduced mass used in the calculation of the reaction rate. At temperatures above ∼1 GK, our rate is lower, for instance, by about 20% around 1.75 GK, because we have re-evaluated the previous data (Isoya et al., Nucl. Phys. 7, 116 (1958)) in a meticulous way. The present interpretation is supported by the direct experimental data. The uncertainties of the present evaluated rate are estimated to be about 20% in the temperature region below 0.2 GK, and are mainly caused by the lack of low-energy experimental data and the large uncertainties in the existing data. Asymptotic giant branch (AGB) stars evolve at temperatures below 0.2 GK, where the ^{19}F(p,α)^{16}O reaction may play a very important role. However, the current accuracy of the reaction rate is insufficient to help to describe, in a careful way, the fluorine over-abundances observed in AGB stars. Precise cross section (or S factor) data in the low energy region are therefore needed for astrophysical nucleosynthesis studies.

Keywords: asymptotic giant branch (AGB) star, nucleosynthesis, astrophysical S factor, cross section, reaction rate

PACS: 21.10.-k, 21.60.Cs, 26.30.+k **DOI:** 10.1088/1674-1137/42/1/015001

1 Introduction

^{19}F is the only naturally occurring stable fluorine isotope. Its abundance is sensitive to the physical conditions of stars [1]. The phenomenon of fluorine over-abundances of factors of 800–8000 has been observed in R-Coronae-Borealis stars, providing evidence for fluorine synthesis in such hydrogen-deficient supergiants [2]. ^{19}F can be produced in the convective zone triggered by a thermal pulse in asymptotic giant branch (AGB) stars [3], which are the main contributors to Galactic fluorine [4]. So far, however, the astronomically observed fluorine over-abundances cannot be understood by using current AGB models, and it seems that additional mixing effects should be involved [5]. It has been shown that deep mixing phenomena in AGB stars could change the stellar outer-layer isotopic composition because of the proton capture reactions, and affect the transported material [6–8]. In this scenario, the main fluorine destruction reaction ^{19}F(p,α)^{16}O possibly plays a role in modifying the fluorine surface abundances [1, 9]. Hydrogen mixing is also important in the model of hydrogen-deficient post-AGB stars, and it can lead to estimates of elemental abundances in better agreement with experimental findings [10].

In terms of nuclear physics, the thermonuclear ^{19}F(p,α)^{16}O reaction rate is still not known sufficiently accurately to address the fluorine over-abundance problem, especially the ^{19}F(p,α_0)^{16}O rate in the low temperature region below 0.2 GK, where it dominates the total ^{19}F(p,α)^{16}O rate. Therefore, a detailed description of fluorine nucleosynthesis is still missing, despite its cru-

Received 11 September 2017, Published online 11 December 2017
∗ Supported by National Natural Science Foundation of China (11490562, 11490560, 11675229) and National Key Research and Development Program of China (2016YFA0400503)
1) E-mail: hejianjun@nao.cas.cn

cial importance.

Figure 1 shows the reaction scheme for the ^{19}F(p,α)^{16}O reaction. This reaction takes place via three different types of channels: (p,α_0), (p,α_π) and (p,α_γ). Hereafter, the group of (p,α_2), (p,α_3) and (p,α_4) accompanying the γ transitions of γ_2, γ_3 and γ_4 is referred to as the (p,α_γ) channel. In this work, we have re-evaluated the cross section data of ^{19}F(p,α_0)^{16}O reactions in the center-of-mass (c.m.) energy region up to 10 MeV. These data are sufficient to account for the thermonuclear ^{19}F(p,α_0)^{16}O reaction rate up to a temperature of 10 GK. Together with the low-energy theoretical predictions for the S factors, a new reaction rate has been derived in the temperature region 0.007–10 GK. Results concerning the other two reaction channels will be the subject of forthcoming papers.

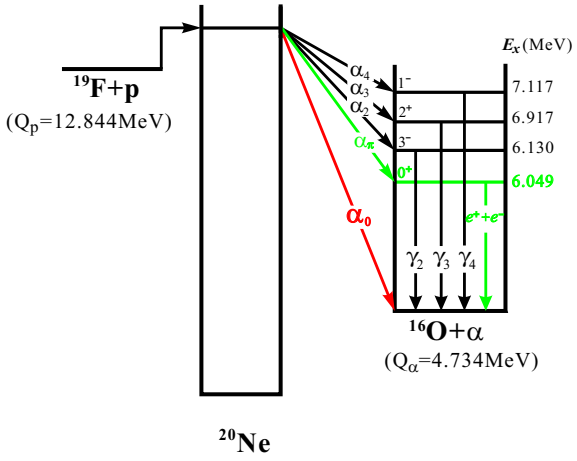

Fig. 1. (color online) Scheme of the ^{19}F(p,α)^{16}O reaction.

2 NACRE compilation

In the Nuclear Astrophysics Compilation of Reaction Rates (NACRE)[1)] [11], ^{19}F(p,α_0)^{16}O astrophysical $S(E)$-factors within $E_{\rm c.m.}$=0.1–10 MeV were recommended on the basis of several works [12–18], where the lowest direct energy point is close to $E_{\rm c.m.}$=461 keV [13]. Figure 2 shows the NACRE compiled S-factor data on a linear scale, where the discrepancies between different data sets can be clearly appreciated. Three major discrepancies need to be pointed out: 1) in the $E_{\rm c.m.}$=1.6–2.5 MeV region, the CLA57 [12] data are different from those of CUZ80 [15]; 2) the resonance energy of the $E_{\rm c.m.}$=1.3 MeV maximum in the cross section is reported to be located at 1.289 MeV in ISO58 [16] and 1.302 MeV in CLA57, with about 13 keV deviation; 3) the BRE59 [13] data are systematically larger than those of ISO58.

3 Data after NACRE

Lombardo et al. reported new direct measurement data [19, 20] on the ^{19}F(p,α_0)^{16}O reaction in the energy region $E_{\rm c.m.}$=0.18–1 MeV. Figure 3 shows the NACRE data together with the new measurements for the ^{19}F(p,α_0)^{16}O, where, for clarity, data in the energy region above 1 MeV are not shown. Here, the extrapolated low-energy non-resonant curves shown in Figs. 2 and 3 are taken from NACRE. It should be noted that: (1) the LOM13 [19] data are systematically larger than those of ISO58 below ~0.75 MeV, but smaller above ~0.85 MeV; (2) the LOM13 and LOM15 [20] data are consistent with BRE59 data within uncertainties, but the latter has very large uncertainties.

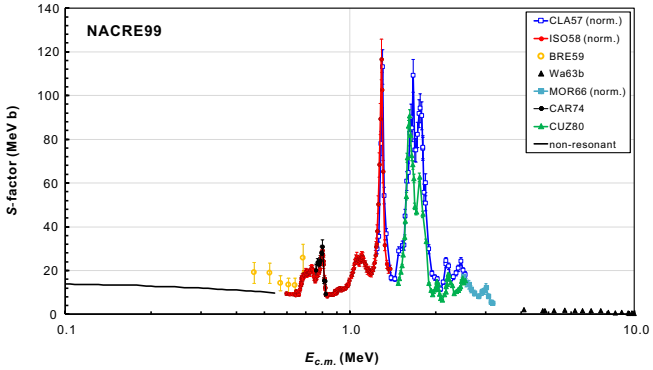

Fig. 2. (color online) Astrophysical S factors of the ^{19}F(p,α_0)^{16}O reaction used in the NACRE compilation [11].

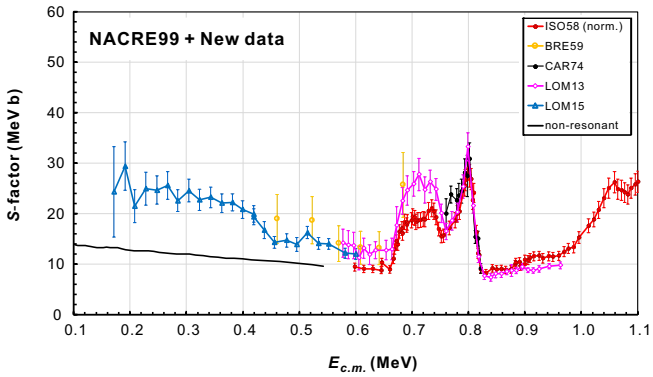

Fig. 3. (color online) Part of astrophysical S factors of the ^{19}F(p,α_0)^{16}O reaction. It includes the data evaluated in the NACRE compilation [11] and new direct measurement data [19, 20]. Here, for clarity, the data within the $E_{\rm c.m.}$=1–10 MeV region are not repeated, as they are exactly the same as in Fig. 2.

La Cognata et al. reported the indirect Trojan horse method (THM) results COG11 [21] and COG15 [22] on this reaction. Starting from the experimentally determined resonance properties, the S factor was deduced by

1) http://pntpm.ulb.ac.be/Nacre/nacre.htm

R-matrix calculations. At temperatures around 0.1 GK, their rate is about 70% larger than the NACRE one, and beyond the previous uncertainties [11]. This difference was owing to the 113 keV resonance. However, their energy resolution was still not enough for a good separation between adjacent resonances. Just recently, a high-resolution THM experiment, IND17 [23], was performed and observed the 251 keV broad resonance clearly. By involving this broad resonance, they obtained a relatively higher S-factor than that of COG15. However, the indirectly measured S factors of IND17 are still lower than the directly measured data of LOM15, although they are in agreement within the relatively large uncertainties (as shown in Fig. 8).

4 Present evaluation

In this work, we have extracted the experimental data or theoretical curves from the figures in the literature by using the GetData Graph Digitizer program[1] (hereafter referred to as "GetData"). Some data are also taken from the Experimental Nuclear Reaction Data (EXFOR) library[2]. We firstly digitized or deduced the ^{19}F(p,α_0)^{16}O cross section data, and then converted to the astrophysical S factors by [24],

$$\sigma(E)=\frac{1}{E}\exp(-2\pi\eta)S(E). \quad (1)$$

The quantity η is called the Sommerfeld parameter and is defined as $\eta=\frac{Z_1Z_2e^2}{\hbar v}$. In numerical units, the exponent is $2\pi\eta=31.29Z_1Z_2\sqrt{\mu/E}$, where the center-of-mass energy E is given in units of keV and the reduced mass μ is in amu. Here, $\exp(-2\pi\eta)$ is the Coulomb barrier penetration probability.

4.1 Astrophysical S factors

The astrophysical S factors have been evaluated in the $E_{\rm c.m.}$=0.1–3.2 MeV region based on the up-to-date experimental data shown in Fig. 4. The higher energy 'WA63b' data [18] shown in Fig. 2 are adopted in the present evaluation. The low energy region of data is expanded in Fig. 5 for clarity. We will discuss the details of our re-evaluation procedure of available data in the following subsections. It should be noted that the solid lines connecting the data points shown in Figs. 2–10 are intended only to guide the eye. Here, the uncertainties of BRE59, MOR66 [17] and CAR74 [14] data are taken from NACRE [11]; those of LOM13 and LOM15 data are taken from Refs. [19, 20] including statistical plus systematical errors; NACRE assumed 3% for CUZ80, while we digitize the errors from Figure 3 of CUZ80; NACRE assumed 7% for ISO58 data, and we assume 10% for these data relative to LOM13 data; NACRE assumed 7% for CLA57 data, and we assume about 12% for these data relative to ISO58 data.

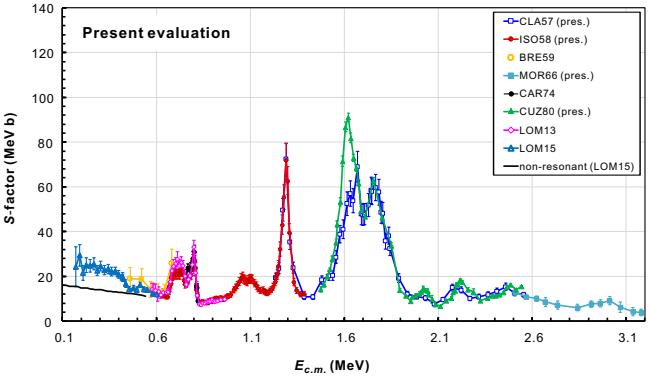

Fig. 4. (color online) Present evaluated astrophysical S factors of the ^{19}F(p,α_0)^{16}O reaction. Data are taken from CLA57 [12], ISO58 [16], BRE59 [13], MOR66 [17], CAR74 [14], CUZ80 [15], LOM13 [19] and LOM15 [20]. The theoretical non-resonant curve is taken from COG15 [22] (i.e., that of NACRE by a scaling factor of 1.16). We have re-evaluated the CLA57, ISO58, MOR66 and CUZ80 data, which are indicated by '(pres.)' in the corresponding legends. The BRE59 data are not used in the present reaction rate calculations due to their large uncertainties. See text for details.

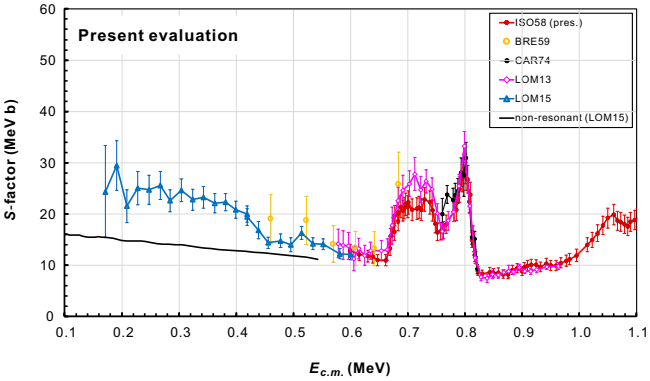

Fig. 5. (color online) Present evaluated astrophysical S factors of the ^{19}F(p,α_0)^{16}O reaction, for the low energy region. Data are taken from CLA57 [12], ISO58 [16], BRE59 [13], MOR66 [17], CAR74 [14], CUZ80 [15], LOM13 [19] and LOM15 [20]. The theoretical non-resonant curve is taken from COG15 [22] (i.e., that of NACRE by a scaling factor of 1.16). We have re-evaluated the CLA57, ISO58, MOR66 and CUZ80 data, which are indicated by '(pres.)' in the corresponding legends. The BRE59 data are not used in the present reaction rate calculations due to their large uncertainties. See text for details.

1) http://getdata-graph-digitizer.com/
2) http://www.nndc.bnl.gov/exfor/exfor.htm

4.1.1 ISO58 data

The ISO58 [16] data evaluated in NACRE are systematically smaller than the BRE59 and LOM13 data below ~0.75 MeV (see Fig. 3), as already mentioned above. To find a possible explanation for such a discrepancy, we have checked the S factors of ISO58 taken from the NACRE website and the Legendre polynomial coefficients in Ref. [16]. Usually, the differential cross section can be reproduced by a Legendre polynomial expansion:

$$\frac{\mathrm{d}\sigma}{\mathrm{d}\Omega}(\theta)=\sum_n B_n P_n(\cos\theta). \quad (2)$$

In this frame, the total cross section can be calculated as $\sigma_{\rm tot}=4\pi B_0$. However, ISO58 expressed their angular distribution by a different equation:

$$\frac{\mathrm{d}\sigma}{\mathrm{d}\Omega}(\theta)=\frac{\lambda\!\!\!^{-2}}{8}\sum_n b_n P_n(\cos\theta), \quad (3)$$

where the additional parameter $\lambda\!\!\!^{-2}$ is inversely proportional to the $E_{\rm c.m.}$ energy. In NACRE, the relative cross sections of ISO58 were normalized to σ=42 mb at the 1.3 MeV resonance. By multiplying the b_0 data (taken from Fig. 4 in Ref. [16]) by a factor of 2.97×10^{-4}, the cross section at the 1.290 MeV resonance peaks at 42 mb, and also $2.97\times10^{-4}\times b_0$ reproduces almost perfectly the ISO58 data evaluated by NACRE over the whole energy range. Therefore, we speculate that NACRE evaluated the ISO58 data by the relation of $2.97\times10^{-4}\times b_0$. In fact, the integrated cross section cannot be estimated by a simple scaling of the b_0 data, and we have to take the energy dependence of $\lambda\!\!\!^{-2}$ reported in Eq. (3) explicitly into account. We performed such a procedure and obtained a new estimate of the integrated cross section starting from the b_0 data of ISO58. In Fig. 6 we show a comparison between our new evaluation of ISO58 data ("ISO58 (Corrected)", in black) and the previous NACRE evaluation ("ISO58 (NACRE)", in light blue). Significant differences appear at the two edges, i.e., the energy regions far away from 1 MeV, and it implies that the energy dependence correction in $\lambda\!\!\!^{-2}$ has a considerable impact on the evaluated cross sections. Finally, the presently evaluated "ISO58 (pres.)" data, which are obtained by multiplying the "ISO58 (Corrected)" data with a normalization factor of 0.8, are consistent with those LOM13, LOM15 and BRE59 data in the whole energy range, as seen in Figs. 4 and 5. It shows that the procedure used here to extract the cross section starting from the ISO58 b_0 data removes the discrepancies between various data sets previously noticed in the $E_{\rm c.m.}$=0.6–1 MeV range.

In the present work, the peak cross section of the 1.3 MeV resonance is evaluated to be (26.0±2.6) mb based on the ISO58 data, much lower than the 42 mb value adopted by NACRE. In fact, there are no absolute cross section values reported in the published literature for this resonant peak. Only Ref. [25] reports a value, 29 mb (with about 15% total uncertainty), which agrees very well with the present value.

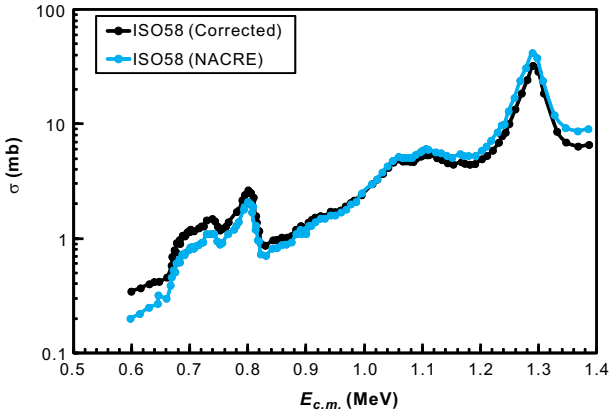

Fig. 6. (color online) Cross sections of the ^{19}F(p,α_0)^{16}O reaction calculated based on the b_0 data of ISO58 [16]. Here, the "ISO58 (Corrected)" data multiplied by a normalization factor of 0.8 equal the presently evaluated "ISO58 (pres.)" data as shown in Figs. 4 and 5.

4.1.2 CLA57 data

In CLA57 [12], the yield of the ground state alpha particles from the ^{19}F(p,α_0)^{16}O reaction was studied in a proton energy range going from 1.3 to 2.7 MeV. The authors analyzed the observed angular distributions in terms of Legendre polynomial expansion (Eq. (1)), and reported the trend of the coefficients as a function of energy. We have obtained the NACRE S-factor data from the NACRE website, and the Legendre polynomial coefficient a_0 of Fig. 4 in Ref. [12] by GetData. We show the data corresponding to $2.51\times10^{-2}\times a_0$ (labelled as "GetData") in Fig. 7 as red dots. We find that they are consistent with the NACRE evaluated data, where the relative cross sections of CLA57 were normalized to σ=42 mb at the 1.3 MeV resonance. However, the two energy scales are slightly different (especially at lower energies, where their difference amounts to about 10 keV in the 1.3 MeV region). The present energy ("GetData") scale can match that of the ISO58 data better. In order to match the present CLA57 data ("GetData") with the ISO58 data evaluated above, the former was multiplied by a factor of 0.63 in our final evaluation (labelled "CLA57 (pres.)" in Fig. 4). In Fig. 4, the shapes of "ISO58 (pres.)" and "CLA57 (pres.)" match very well around the 1.3 MeV resonance, where the values of the evaluated S factor are 72.1 MeV·b for ISO58 at 1.290 MeV, and 72.4 MeV·b for CLA57 at 1.292 MeV. The peak cross sections for six resonances listed in Table IV in Ref. [12] are also shown in Fig. 7 for comparison. These data were determined relative to the known ^{19}F(p,α_γ)^{16}O cross section. It shows they are roughly consistent with

the NACRE and the present results within their large uncertainties, except for two data points at 2.01 and 2.45 MeV. However, most of these data are much larger than the present evaluation if considering the above factor of 0.63 for "GetData" in Fig. 7. Therefore, we conclude that these peak cross sections data listed in Table IV in Ref. [12] are unreliable.

In fact, CLA57 derived a value of 46 mb at the $E_{\rm p}$=1.358 MeV resonance by normalizing their results to a previously uncertain (p,α_γ) value at the 1.372 MeV resonance (i.e., 300 mb estimated by Streib et al. [26]). By considering the above normalization factor of 0.63, a value of 29 mb (=46×0.63) is obtained, which is consistent with the present evaluated value of 26 mb.

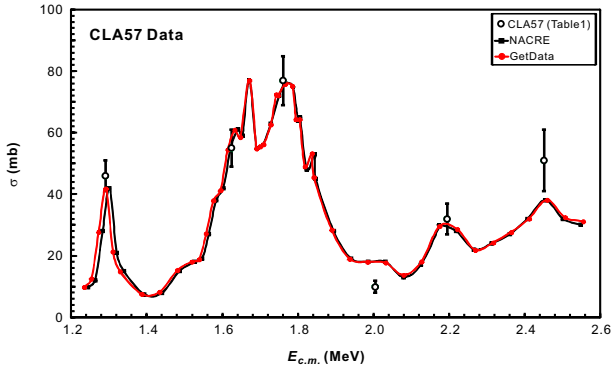

Fig. 7. (color online) Cross sections of the ^{19}F(p,α_0)^{16}O reaction starting from the data reported by CLA57 [12].

4.1.3 CUZ80 data

In the NACRE compilation, the data of Fig. 3 in CUZ80 [15] were digitized as shown in Figs. 2 and 3. However, they simply adopted only about 3% uncertainty on the data. In this work, we adopted the NACRE evaluated data, while the associated uncertainties were digitized from Fig. 3 in CUZ80. Uncertainties vary, depending on the energy, from about 2% up to 20%. The present evaluation is indicated as "CUZ80 (pres.)" in Fig. 4. In the $E_{\rm c.m.}$=1.52–1.65 MeV region, the "CUZ80 (pres.)" data are considerably different from those of "CLA57 (pres.)". Therefore, new experiments are needed to clarify this discrepancy.

4.1.4 MOR66 data

In MOR66 [17], the coefficients of the Legendre polynomials were obtained at six energy points as listed in their Table I. By using the coefficient A_0, NACRE normalized the data of MOR66 at 2.507 MeV to σ=28 mb, the averaged value of CLA57 and CUZ80 (see Fig. 2). In order to match the "CLA57 (pres.)" data, we have normalized the MOR66 data at 2.507 MeV to σ=20.8 mb, labelled as "MOR66 (pres.)" in Fig. 4.

4.1.5 Low-energy extrapolation

In NACRE, a non-resonant contribution was calculated below 0.46 MeV for s-wave capture with the procedure described in Ref. [27], and then adjusted to the lower experimental points in the 0.46≤$E_{\rm c.m.}$≤0.60 MeV range. This non-resonant contribution matches the old NACRE "ISO58 (norm.)" data well, as shown in Fig. 2. In this work, we have adopted the non-resonant contribution fitted in the R-matrix calculations of LOM15, i.e., the NACRE non-resonant contribution with a scaling factor of 1.16, as shown in Figs. 4 and 5.

In addition, the low-energy unpublished experimental data and theoretical predictions for the ^{19}F(p,α_0)^{16}O reaction have been reviewed in Ref. [28]. In the unpublished thesis work of LOR78 [29], differential cross sections were measured in the energy range between $E_{\rm p}$=0.14–0.90 MeV at the two angles $\theta_{\rm lab}$=90° and 135°. Relative angular distributions were measured at four proton energies: 250, 350, 450 and 550 keV. The astrophysical S factor was parameterized in the analytical form [24]

$$S(E)=S(0)+S'(0)E+\frac{1}{2}S''(0)E^2, \qquad (4)$$

with $S(0)$=3.77 MeV·b, $S'(0)$=-5.13 b and $S''(0)$=90.75 b·MeV^{-1}, by simply assuming $\sigma_{\rm tot}=4\pi\frac{{\rm d}\sigma}{{\rm d}\Omega}(90°)$. Later, HER91 [30] and YAM93 [31] independently performed zero and finite-range Distorted Wave Born Approximation (DWBA) analysis of the LOR78 data. Two calculated astrophysical S factors agree within ∼15%. Based on the predicted angular distribution, HER91 quoted an S factor ($S(0)$=8.755 MeV·b, $S'(0)$=-3.48 b and $S''(0)$=20.1 MeV^{-1}b) about a factor of two larger than the LOR78 one at low energies, as shown in Fig. 8. As commented on in NACRE, HER91 and YAM93 were focused mainly on the relative energy dependence of the cross section, without accurate checks on the absolute cross sections, which may be underestimated by a factor of 2. In fact, the underestimation of LOR78 data in Fig. 10 is obvious. Therefore, it seems reasonable that the unpublished LOR78 data were not included in the NACRE compilation.

Figure 8 shows a comparison between different predictions. The HER91 result is still about a factor of 2 smaller than the presently re-evaluated non-resonant contribution. In addition, the R-matrix results of LOM15 based on direct experimental data, as well as those of COG15 and IND17 based on indirect THM data, are also shown in Fig. 8. The recent result of IND17 is quite close to that of LOM15, except in the energy region around 0.2∼0.4 MeV, although both results are roughly consistent within the large uncertainties. For clarity, only the centroid value of IND17 is shown, and actually an uncertainty of 16% was assumed in their work. As evident from the figure, we are still lack experimental data in the energy region below 0.2 MeV, and the existing

data around 0.2 MeV are not sufficiently accurate yet. Therefore, precise direct cross-section measurements are of great importance to describe proton-induced fluorine destruction in astrophysical nucleosynthesis studies.

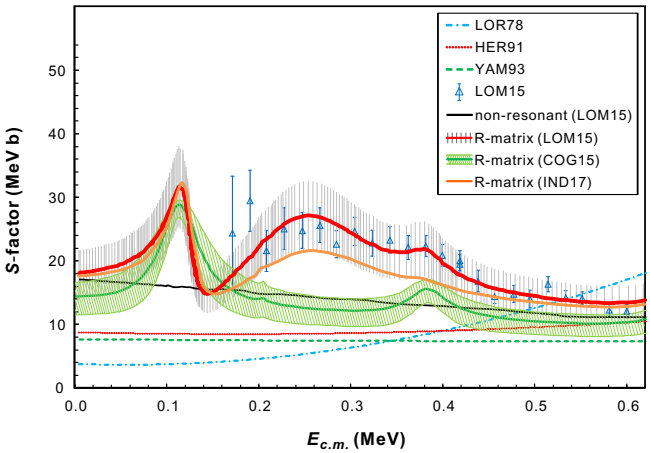

Fig. 8. (color online) Low-energy astrophysical S factors of the ^{19}F(p,α_0)^{16}O reaction. The non-resonant predictions (LOR78 [29], HER91 [30], YAM93 [31] and LOM15 [20]) and R-matrix results (COG15 [22], IND17 [23], and LOM15) are shown for comparison.

4.2 Angular distribution

In general, experimentally observed angular distributions can be fitted in two different ways: (1) the Legendre polynomials, from Eq. 2 above; or (2) the cosine polynomials, which can be expressed as

$$\frac{\mathrm{d}\sigma}{\mathrm{d}\Omega}(\theta)=\sum_n A_n\cos^n\theta. \tag{5}$$

It can easily be shown that the total cross section can be deduced by the differential cross section at θ=90° and the presently defined angular distribution factor f with the equation:

$$\sigma_{\rm tot}=4\pi\times\frac{\mathrm{d}\sigma}{\mathrm{d}\Omega}(90^\circ)\times f. \tag{6}$$

The factor f can be calculated with the coefficients of Legendre polynomials B_i (up to 4$^{\rm th}$ order) by

$$f=1\Big/\left(1-\frac{B_2}{2B_0}+\frac{3B_4}{8B_0}\right), \tag{7}$$

with $\sigma_{\rm tot}=4\pi B_0$. Alternatively, this f can be calculated with the coefficients of cosine polynomials A_i (up to 4$^{\rm th}$ order) by

$$f=1+\frac{A_2}{3A_0}+\frac{A_4}{5A_0}, \tag{8}$$

with $\sigma_{\rm tot}=4\pi A_0\times f$. Here, Eqs. (5)–(8) are valid either in the c.m. or the lab. frame, and obviously f is independent of the coordinate frame. For the ^{19}F(p,α_0)^{16}O reaction, the difference between c.m. and lab. differential cross sections is quite small, about 1% at ~90° in the energy region studied. This difference can be neglected if compared to the uncertainty of experimental data.

One or two kinds of expansion coefficients were given in the previous works, and their relation was deduced in Ref. [32]. By using these coefficients, we have plotted the factor f in Fig. 9. It shows that the factor f assumes large values in regions corresponding to resonances, while the non-resonant region has a factor around 1. As a conclusion, to give an approximate estimate of the non-resonant part of the cross section, one can measure the differential cross section at $\theta_{\rm lab}$=90°, and then by multiplying by a factor of 4π, the total cross section can be determined (see Eq. (6)). This method can simplify lengthy angular distribution measurements if one needs to know the behavior of the total cross section far from a resonant peak. There are still some discrepancies between different datasets as seen in Fig. 9, which should be resolved where necessary. In addition, the angular distribution factors (f) below 0.6 MeV are not exactly 1 (about 0.8~1.2), implying there are some resonances in this region which were actually observed by LOM15. This also demonstrates that the previous non-resonance extrapolation set only rough lower limits. Since there is a resonance around 0.113 MeV as shown in Fig. 8, a future experiment should measure either angular distribution or total cross section.

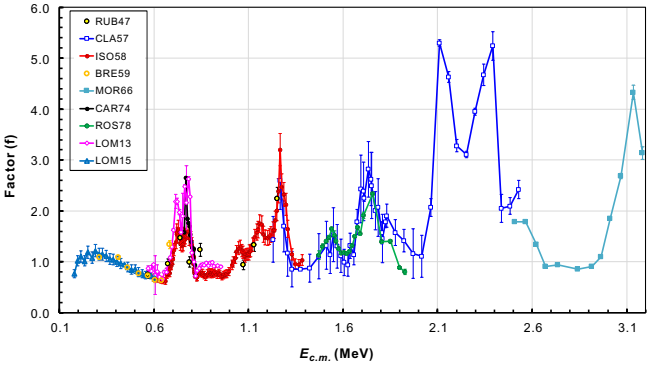

Fig. 9. (color online) Angular distribution factor f as a function of energy for the ^{19}F(p,α_0)^{16}O reaction.

4.3 Differential cross section

We have re-evaluated the differential cross sections observed at $\theta_{\rm lab}$=90° as shown in Fig. 10. Here, the $E_{\rm c.m.}$ energy scale has been corrected for the energy loss in the target. For the differential cross section dσ/dΩ(90°), DIE80 [33] obtained an absolute measured value of (1.05±0.09) mb/sr at $E_{\rm p}$=1.354 MeV (with ~1 keV target energy loss), while LER69 [34], in a dedicated series of experiments, obtained an absolute measured value of (1.02±0.10) mb/sr at $E_{\rm p}$=1.360 MeV (with ~7–24 keV target energy loss). These peaks are actually due

to the same resonance, after taking the target energy-loss effect into account, and they give rise to the peak at $E_{\rm c.m.}$=1.280 MeV shown in Fig. 10. Because there are no other absolute measurements available in this energy region, here we adopted the DIE80 excitation function as the reference. The ISO58 and RAN58 [35] data have been normalized to DIE80 with factors of 0.5 and 0.7, respectively. The results show that the ISO58 and DIE80 data are consistent down to about 0.8 MeV, below which they behave quite differently.

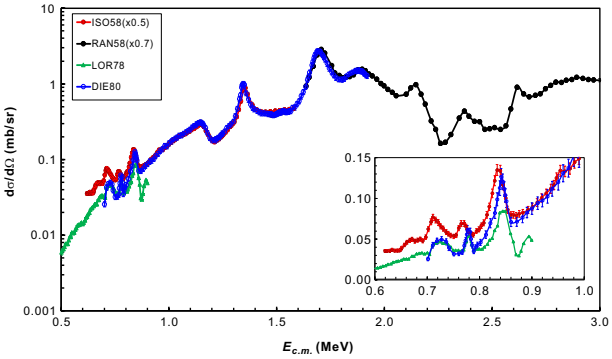

Fig. 10. (color online) Evaluation of ^{19}F(p,α_0)^{16}O differential cross sections observed at $\theta_{\rm lab}$=90°. "ISO58(×0.5)" data are obtained by multiplying the digitized Fig. 2 data in Ref. [16] by a correction factor of 0.5. "RAN58(×0.7)" data are obtained by multiplying the digitized Fig. 2 data in Ref. [35] by a factor of 0.7. "DIE80" is the reference, as discussed in the text. The original unpublished LOR78 data are shown for comparison. The enlarged small figure is inserted for clarity (in linear scale).

As mentioned above, a normalization factor of 0.5 is adopted for the observed ISO58 data (i.e., Fig. 2 data in Ref. [16]). The rationality of this normalization factor will be explained below. Firstly, we extracted the coefficients (b_0, b_2 and b_4) of the Legendre polynomials from Fig. 4 in ISO58, and then calculated the angular distribution factor f by using Eq. 7. Finally we calculated the differential cross sections by the following relation, as discussed above:

$$\frac{{\rm d}\sigma}{{\rm d}\Omega}(90^\circ)=\frac{1}{4\pi f}\times\left(\frac{2.97\times10^{-4}\times b_0}{E_{\rm c.m.}}\times0.8\right), \qquad (9)$$

where the term in the parenthesis represents the total cross section with a normalization factor of 0.8 used in Sec. 3.1.1 for the ISO58 S-factor data. Figure 11 shows a comparison between the two datasets. It shows that they are very consistent, and the normalized ISO58 data are highly consistent with the DIE80 data (except the region below 0.8 MeV) as shown in Fig. 10. In order to make both ISO58 S-factor and differential cross section data consistent with other datasets simultaneously, the differential cross sections shown in Fig. 2 of ISO58 should be reduced by a factor of 0.5 (possibly due to a mistake). In fact, this normalization factor of 0.5 is a kind of "correction" factor.

In addition, the RAN58 derived a total ^{19}F(p,α_0)^{16}O cross section value of 40 mb at the $E_{\rm p}$=1.35 MeV resonance, based on the CLA57 angular distribution. By considering the above normalization factor of 0.7, a value of 28 mb (=40×0.7) is obtained, which is consistent with the present evaluated value of (26.0±2.6) mb.

There are large discrepancies among ISO58, LOR78 and DIE80 data in the region below 0.8 MeV, as shown in the insert plot in Fig. 10. Roughly speaking, the LOR78 data are about a factor of 2 smaller than ISO58(×0.5), and we do not know the exact origin of this discrepancy. Here, the unpublished LOR78 data have not been included in the present evaluation. This underestimation is possibly owing to target degradation, since LOM78 used a very strong proton beam of up to 200 μA. Recently, we have tested many CaF_2 and LiF targets, and found that target degradation was very serious with a proton beam of several μA [36]. In addition, the exact reason why DIE80 is different from ISO58(×0.5) below about 0.84 MeV is also unknown. Here we assume that it can again be attributed to target degradation. In DIE80, it is described that "beam currents were around 1 μA, on a 1 mm^2 spot" . At low energies the cross section becomes small, and the machine time on the target should be longer than in the higher energy region. This very sharp beam bombarding a very thin LiF target (5.3 μg/cm^2 of F) during a long run could seriously degrade the target, which is possibly why the DIE80 differential cross section reduced considerably. In the ISO58 experiment, on the other hand, the proton beam bombarded a 50 μg/cm^2 CaF_2 target with currents of 0.4 to 2 μA, where a beam defining slit of 3.3 mm was utilized "to insure durability

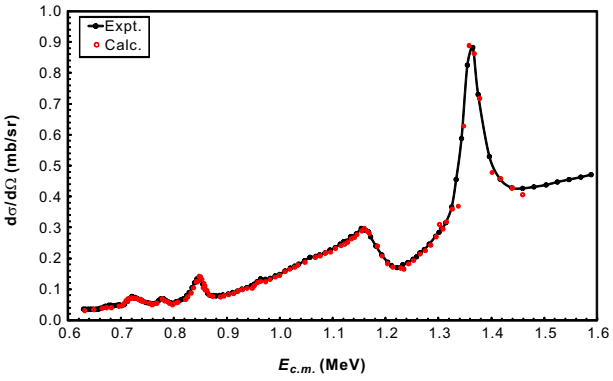

Fig. 11. (color online) Differential cross sections of the ^{19}F(p,α_0)^{16}O reaction at $\theta_{\rm lab}$=90° evaluated based on the ISO58 data [16]. Here, "Expt." represents exactly the results of "ISO58(×0.5)" shown in Fig. 10, and "Calc." represents the calculated results from Eq. 9, as explained in the text.

of the target under the ion bombardment by reducing the current density". The much thicker CaF_2 target and reduced current density could alleviate the impact of target degradation on the results.

5 Reaction rates

It is well-known that the reaction rate of charged-particle induced reactions can be calculated, in terms of astrophysical S factor, by the following equation [11, 24]:

$$N_A\langle\sigma v\rangle = N_A\left(\frac{8}{\pi\mu}\right)^{1/2}\frac{1}{(kT)^{3/2}} \times\int_0^\infty S(E)\exp\left[-\frac{E}{kT}-2\pi\eta\right]\mathrm{d}E. \quad (10)$$

As already discussed in Eq. 4, the reduced mass μ is in units of amu, and it enters into the exponential term in the above equation. In the present work, μ is precisely calculated with proton mass of 1.007825u, and ^{19}F mass of 18.998403u [37]. If one simply approximates proton and ^{19}F mass as 1u, and 19u, respectively, the calculated penetration factor of exp(-2$\pi\eta$) will be different from the precise one. Such an impact is shown clearly in Fig. 12, where the approximated factor is enhanced considerably in the low energy region. In other words, the approximation of mass values can considerably affect the reaction rate in the low temperature region.

The thermonuclear ^{19}F(p,α_0)^{16}O rate has been calculated by numerical integration of our evaluated S factors with Eq. 10. We divided the evaluated ^{19}F(p,α_0)^{16}O S-factor datasets into the following three regions: (1) in the low energy region where no experimental data are available, we adopt the theoretical R-matrix results of LOM15 as shown in Fig. 8 (with assumed uncertainty of 20% [20]); (2) in the higher energy region of $E_{\rm c.m.}$=4–10 MeV, the NACRE 'WA63b' data [18] shown in Fig. 2 are adopted (with assumed uncertainty of 20% [11]); (3) in the energy region of $E_{\rm c.m.}$=0.2–3.2 MeV, we adopt the evaluated data and associated errors in Fig. 4, except for the BRE59 data (because of their large uncertainties). It should be noted that there are discrepancies between the CLA57 and CUZ80 data, as shown in Fig. 4, and hence we adopt the average of the two datasets in the reaction rate calculations, although the maximum difference resulting in the rate is less than 9% (smaller than 3% below 2 GK). Additionally, we assumed a ±2 keV uncertainty of the experimental $E_{\rm c.m.}$ energies (shown in Fig. 4) in the numerical integration, but this uncertainty results in no more than 3% uncertainty on the lower and upper limits. The numerical values of the present reaction rate and the associated lower and upper limits are listed in Table 1. Finally, the present rate is parameterized by the standard format of [38]:

$$\begin{aligned} N_A\langle\sigma v\rangle = {} & \exp(51.8361-\frac{9.79933}{T_9}+\frac{315.811}{T_9^{1/3}}-366.895T_9^{1/3}+16.2212T_9-0.863T_9^{5/3}+210.485\ln T_9) \\ & +\exp(48.7403-\frac{0.031187}{T_9}-\frac{11.441}{T_9^{1/3}}-32.2709T_9^{1/3}+3.34216T_9-0.2476T_9^{5/3}+8.72415\ln T_9) \\ & +\exp(6165.89-\frac{2.56546}{T_9}+\frac{759.439}{T_9^{1/3}}-9936.72T_9^{1/3}+6431.65T_9-5224.7T_9^{5/3}+1610.12\ln T_9), \end{aligned} \quad (11)$$

with a fitting error of less than 1.5% over the entire temperature region of 0.007–10 GK.

A comparison between different rates relative to the present rate is shown in Fig. 13. The differences between LOM15, IND17 and NACRE reaction rates were already discussed before, and will not be repeated here. Figure 13 shows that our rate is lower than all the previous rates above ~1 GK, owing to the present smaller evaluated ISO58 and CLA57 S factors. Within the large uncertainties ((10~20)% for the present, 20% [20] for LOM15 and 16% [23] for IND17), our rate is consistent with the LOM15 and IND17 rates, but it is larger than the NACRE one when below 1 GK (where a small non-resonant S-factor was assumed in the low energy region). Furthermore, Fig. 13 shows that our rate is smaller than the IND17 rate in the low temperature region (e.g., by up to about 20% around 0.007 GK). Since the low energy part of the S-factor quoted in IND17 is quite similar to the present one, we believe that the main source leading

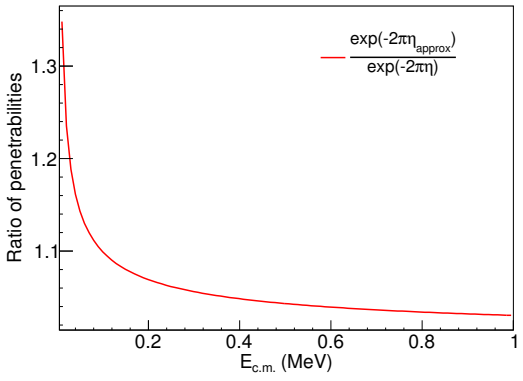

Fig. 12. (color online) Ratio of penetration factor exp(-2$\pi\eta$) by using precise and approximated Sommerfeld parameter η for the ^{19}F+p system. Here the parameters η and $\eta_{\rm approx}$ are calculated respectively by using the precise and the approximate value of the reduced mass μ. See text for details.

Table 1. Thermonuclear ^{19}F(p,α_0)^{16}O reaction rate associated with the lower and upper limits (in units of cm^{3}s^{-1}mol^{-1}).

T_9	rate	lower limit	upper limit
0.007	6.161E-29	4.929E-29	7.393E-29
0.008	3.490E-27	2.792E-27	4.189E-27
0.009	1.058E-25	8.468E-26	1.270E-25
0.010	1.999E-24	1.599E-24	2.399E-24
0.011	2.610E-23	2.088E-23	3.132E-23
0.013	1.937E-21	1.549E-21	2.324E-21
0.015	6.409E-20	5.127E-20	7.691E-20
0.018	4.353E-18	3.482E-18	5.224E-18
0.020	4.434E-17	3.548E-17	5.321E-17
0.025	4.645E-15	3.716E-15	5.574E-15
0.030	1.618E-13	1.295E-13	1.942E-13
0.040	2.897E-11	2.318E-11	3.477E-11
0.050	1.185E-09	9.481E-10	1.422E-09
0.060	2.034E-08	1.627E-08	2.441E-08
0.070	1.948E-07	1.558E-07	2.338E-07
0.080	1.224E-06	9.790E-07	1.470E-06
0.090	5.639E-06	4.505E-06	6.773E-06
0.100	2.064E-05	1.647E-05	2.481E-05
0.110	6.371E-05	5.076E-05	7.666E-05
0.140	9.585E-04	7.643E-04	1.153E-03
0.180	1.368E-02	1.112E-02	1.623E-02
0.200	3.932E-02	3.241E-02	4.622E-02
0.250	3.219E-01	2.738E-01	3.699E-01
0.300	1.560E+00	1.358E+00	1.763E+00
0.350	5.386E+00	4.762E+00	6.010E+00
0.400	1.470E+01	1.314E+01	1.627E+01
0.450	3.390E+01	3.049E+01	3.730E+01
0.500	6.891E+01	6.225E+01	7.557E+01
0.600	2.184E+02	1.980E+02	2.388E+02
0.700	5.446E+02	4.935E+02	5.958E+02
0.800	1.159E+03	1.048E+03	1.270E+03
0.900	2.200E+03	1.984E+03	2.415E+03
1.000	3.833E+03	3.450E+03	4.216E+03
1.250	1.183E+04	1.060E+04	1.304E+04
1.500	2.867E+04	2.560E+04	3.166E+04
1.750	5.973E+04	5.303E+04	6.602E+04
2.000	1.115E+05	9.831E+04	1.233E+05
2.500	3.011E+05	2.623E+05	3.330E+05
3.000	6.287E+05	5.434E+05	6.947E+05
3.500	1.094E+06	9.407E+05	1.207E+06
4.000	1.672E+06	1.434E+06	1.842E+06
5.000	3.037E+06	2.599E+06	3.338E+06
6.00	4.506E+06	3.855E+06	4.948E+06
7.00	5.898E+06	5.045E+06	6.475E+06
8.00	7.156E+06	6.120E+06	7.860E+06
9.00	8.257E+06	7.060E+06	9.079E+06
10.00	9.203E+06	7.865E+06	1.013E+07

to the disagreement between the present and IND17 data sets at very low T_9 values could be the rough approximation of the reduced mass value in IND17. In this context, it is worth noting that effects due to use of an approximated reduced mass value are almost canceled out when one reports ratio of reactions rates calculated under the same approximation. In the temperature region of 0.007∼1 GK, our rate is almost identical to that of LOM15 since we adopted a similar S factors at low energies. The small differences originate from the fact that we adopt the experimental S-factor data at energies below 0.8 MeV, while LOM15 adopted the R-matrix predictions in the same energy region. This is why one may see a small bump (about 8%) around 0.2 GK in Fig. 13, due to a bump structure observed around 0.185 MeV shown in Fig. 8, where no such structure was predicted by the LOM15's R-matrix calculation. The uncertainties of the present low temperature rate are estimated to be ∼20%, which are mainly determined by the large uncertainties adopted for the R-matrix calculations (20% assumed in Ref. [20]) and those of the experimental data.

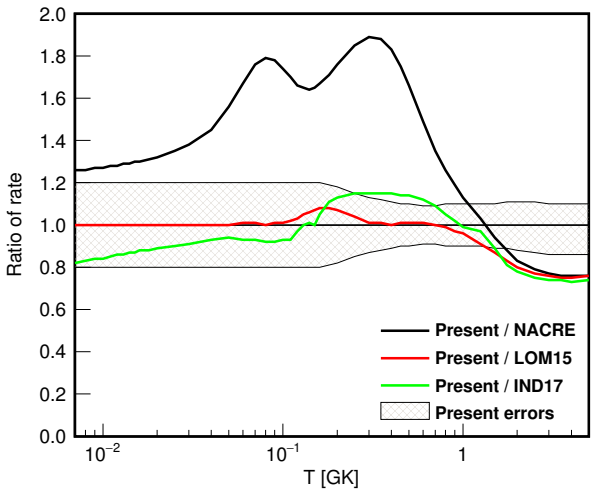

Fig. 13. (color online) ^{19}F(p,α_0)^{16}O reaction rate ratios between the present and NACRE [11], LOM15 [20], IND17 [23] rates. The associated error of the present rate is shown as the cross-hatched band.

6 Summary and outlook

We have re-evaluated the available astrophysical S factors of the ^{19}F(p,α_0)^{16}O reaction in the energy region of $E_{\rm c.m.}$=0.2–3.2 MeV. A thermonuclear ^{19}F(p,α_0)^{16}O reaction rate in the temperature region of 0.007–10 GK has been calculated based on these evaluated data and the low-energy theoretical R-matrix extrapolation. The results show that our new rate is lower than the previously reported value [23] at temperatures below ∼0.2 GK, e.g., by up to about 20% around 0.01 GK; this effect seems to be due to an approximation used in the previous numerical integration. Furthermore, our rate is lower at temperatures above ∼1 GK, e.g., by about 20% around 1.75 GK, mainly because we have re-evaluated

the previous data of Ref. [16], which had not been interpreted correctly in the previous NACRE compilation. The present interpretation is supported by direct experimental data. However, the (p,α_γ) channel dominates the total rate in the temperature above ∼0.2 GK, and hence such lowering in the (p,α_0) rate does not appreciably change the total rate. The present rate uncertainties are still large, about 20% in the low temperature region of 0.007–0.2 GK, where the (p,α_0) channel dominates the total $^{19}F(p,\alpha)^{16}O$ rate. This temperature region corresponds to an energy $E_{c.m.}$ below ∼240 keV, where the precise experimental cross section (or S factor) data are strongly required for astrophysical nucleosynthesis studies in AGB stars. In addition, we find large discrepancies between different studies of the 90° differential cross sections below 0.9 MeV, which also needs further experimental clarification.

In 2014, the National Natural Science Foundation of China (NSFC) approved the Jinping Underground Nuclear Astrophysics laboratory (JUNA) project [39], which aims at direct cross-section measurements of four key stellar nuclear reactions right down to the Gamow windows. In order to solve the observed fluorine overabundances in AGB stars, measuring the key $^{19}F(p,\alpha)^{16}O$ reaction at effective burning energies (i.e., at Gamow window of $E_{c.m.}$=70–350) has been established as one of the scientific research sub-projects [40], with the accuracy required by the stellar model calculations. We hope that the new direct experimental data will help resolve the element abundances problem as well as the heavy-element nucleosynthesis scenario, by putting various astrophysical models on a firmer experimental ground.

References

1 S. Lucatello et al, Astrophys. J., **729**: 40 (2011)
2 G. Pandey, D. L. Lambert, and R. N. Kameswara, Astrophys. J., **674**: 1068–1077 (2008)
3 S. Cristallo et al, Astrophys. J., **696**: 797–820 (2009)
4 A. Jorissen, V. V. Smith and D. L. Lambert, Astron. Astrophys., **261**: 164–187 (1992)
5 M. Lugaro et al, Astrophys. J., **615**: 934–946 (2004)
6 K. M. Nollett, M. Busso, and G. J. Wasserburg, Astrophys. J., **582**: 1036–1058 (2003)
7 M. L. Sergi et al, Phys. Rev. C, **82**: 032801R (2010)
8 M. Busso et al, Astrophys. J., **717**: L47–L51 (2010)
9 C. Abia et al, Astrophys. J., **737**: L8 (2011)
10 G. C. Clayton et al, Astrophys. J., **662**: 1220–1230 (2007)
11 C. Angulo et al, Nucl. Phys. A, **656**: 3–183 (1999)
12 R. L. Clarke and E.B. Paul, Can. J. Phys., **35**: 155–167 (1957)
13 G. Breuer, Z. Phys., **154**: 339–351 (1959)
14 R. Caracciolo et al, Lett. Nuovo Cim., **11**: 33–38 (1974)
15 P. Cuzzocrea et al, Lett. Nuovo Cim., **28**: 515–522 (1980)
16 A. Isoya, H. Ohmura, and T. Momota, Nucl. Phys., **7**: 116–125 (1958)
17 S. Morita et al, J. Phys. Soc. Japan, **21**: 2435–2438 (1966)
18 K. L. Warsh, G. M. Temmer, and H. R. Blieden, Phys. Rev., **13**: 1690–1696 (1963)
19 I. Lombardo et al, J. Phys. G: Nucl. Part. Phys., **40**: 125102 (2013)
20 I. Lombardo et al, Phys. Lett. B, **748**: 178–182 (2015)
21 M. La Cognata et al, Astrophys. J., **739**: L54 (2011)
22 M. La Cognata et al, Astrophys. J., **805**: 128 (2015)
23 I. Indelicato et al, Astrophys. J., **845**: 19 (2017)
24 C. E. Rolfs and W. S. Rodney, *Cauldrons in the Cosmos* (Chicago: Univ. of Chicago Press, 1988)
25 P. Cuzzocrea et al, Report INFN/BE-80/5 (1980)
26 J. F. Streib, W. A. Fowler, and C. C. Lauritsen, Phys. Rev., **59**: 253 (1941)
27 C. Y. Chao, Phys. Rev., **80**: 1035–1042 (1950)
28 M. Wiescher, J. Görres, and H. Schatz, J. Phys. G: Nucl. Part. Phys., **25**: R133–R161 (1999)
29 H. Lorentz-Wirzba, PhD thesis, Univ. Müster, 1978
30 H. Herndl et al, Phys. Rev. C, **44**: 952R–955R (1991)
31 Y. Yamashita and Y. Kudo, Prog. Theor. Phys., **90**: 1303–1310 (1993)
32 A. Isoya, K. Goto, and T. Momota, J. Phys. Soc. Japan, **11**(9): 899–906 (1956)
33 D. Dieumegard, B. Maurel, and G. Amsel, Nucl. Instr. Meth., **168**: 93–103 (1980)
34 G. M. Lerner and J. B. Marion, Nucl. Instr. Meth., **69**: 115–121 (1969)
35 W. A. Ranken, T. W. Bonner, J. H. McCrary, Phys. Rev., **109**: 1646–1651 (1958)
36 L. Y. Zhang, S. W. Xu, J. J. He et al, under preparation
37 M. Wang et al, Chin. Phys. C, **41**: 030003 (2017)
38 T. Rauscher and F.-K. Thielemann, At. Data Nucl. Data Tables, **75**: 1–351 (2000)
39 W. P. Liu et al, Sci. China-Phys. Mech. Astron., **59**: 642001 (2016)
40 J. J. He et al, Sci. China-Phys. Mech. Astron., **59**: 652001 (2016)